Metals **2015**, *5*, 1704-1716; doi:10.3390/met5031704

OPEN ACCESS

metals

ISSN 2075-4701

www.mdpi.com/journal/metals/

Article

Characterization of Microstructure and Mechanical Properties of Resistance Spot Welded DP600 Steel

Ali Ramazani [1,*], Krishnendu Mukherjee [2], Aydemir Abdurakhmanov [3], Mahmoud Abbasi [4] and Ulrich Prahl [2]

[1] Department of Chemical Engineering, University of Michigan, Ann Arbor, MI 48109, USA

[2] Department of Ferrous Metallurgy, RWTH Aachen University, Aachen 52072, Germany; E-Mails: krishnendu.mukherjee789@googlemail.com (K.M.); ulrich.prahl@iehk.rwth-aachen.de (U.P.)

[3] Welding and Joining Institute, RWTH Aachen University, Aachen 52072, Germany; E-Mail: aydemir.abdurakhmanov@requisimus.com

[4] Faculty of Engineering, University of Kashan, Kashan-8731751167, Iran; E-Mail: abbaci.m@gmail.com

* Author to whom correspondence should be addressed; E-Mail: ramazani@umich.edu; Tel.: +1-734-353-3569; Fax: +1-734-763-0459.

Academic Editor: Hugo F. Lopez

Received: 9 July 2015 / Accepted: 13 September 2015 / Published: 17 September 2015

Abstract: Resistance spot welding (RSW) as a predominant welding technique used for joining steels in automotive applications needs to be studied carefully in order to improve the mechanical properties of the spot welds. The objectives of the present work are to characterize the resistance spot weldment of DP600 sheet steels. The mechanical properties of the welded joints were evaluated using tensile-shear and cross-tensile tests. The time-temperature evolution during the welding cycle was measured. The microstructures observed in different sites of the welds were correlated to thermal history recorded by thermocouples in the corresponding areas. It was found that cracks initiated in the periphery region of weld nuggets with a martensitic microstructure and a pull-out failure mode was observed. It was also concluded that tempering during RSW was the main reason for hardness decrease in HAZ.

Keywords: resistance spot welding; dual-phase steel; microstructure; tensile-shear test; cross-tensile test; hardness map; fracture

1. Introduction

The main focus of the automotive industry is to reduce the weight of car, enhance safety and crashworthiness while the cost is low [1–3]. In comparison with traditional low carbon and high strength low alloy steels, dual phase (DP) steels provide a combination of good formability and strength [4,5]. DP steels are attractive to automakers as they can offer safety, affordability, fuel efficiency, and environmental responsibility [6–8]. Wang *et al.* [9] studied the high strain rate behavior of high strength DP steels. They reported that for high strain rate tests, comparable to crash situations, the DP steels fail in ductile mode. The microstructure of DP steel consists of hard martensite particles dispersed in a soft, ductile ferrite matrix. A well-balanced ratio between ferrite and martensite volume fractions has been reported to be the most important factor affecting the mechanical properties of DP steels [10,11]. The other factors affecting the mechanical behavior includes: the morphology of the martensite islands, carbon content in the martensite, and the deformation condition of ferrite, *i.e.*, dislocation density [12,13].

Welding is the most important joining technique in the automotive industry, and its condition plays a prominent role in determining the final mechanical properties of the joints. Local heat input from the welding heat source induces a large temperature gradient on the workpiece and it may destroy the microstructure and hence the mechanical properties of steels [14]. This holds in particular for DP steels which contain a specific ferritic-martensitic microstructure [15,16]. It is, therefore, important to characterize the microstructure evolution during welding and its influence on the final mechanical properties of DP steels.

Resistance Spot Welding (RSW) is the primary sheet metal welding process in the manufacture of automotive assemblies [17]. The embedded infrastructure makes RSW an economically-desirable process. The failure modes of steel RSWs are button pull-out, partial pull-out, and interfacial fracture, where the button pull-out is preferred as more energy is absorbed during this kind of failure [18]. Zhang *et al.* [19] reported that the failure mode primarily depends on the fusion zone size and failure tends to occur under pull-out mode as fusion zone size increases. Ma *et al.* [20] reported about the formation of shrinkage voids in fusion zone of spot-welded DP600 steel. According to them, these voids are formed due to rich chemistry of DP steels as compared to low carbon steels.

According to the industrial standards, the minimum size of the spot welds to guarantee the pull-out fracture follows the relation $D = K\sqrt{t}$, where D is the weld nugget diameter in mm, K is a process-dependent constant ranging from 3 to 6, and t is the minimum sheet thickness in mm [21,22].

Pouranvari *et al.* [23] discussed a new criterion to ensure button pull-out failure for advanced high strength steels. Khan *et al.* [24] studied the effects of alloying elements and processing techniques on failure modes of AHSS steels RSWs. They concluded that steels with higher carbon content had higher FZ hardness demonstrating a strong relationship between chemistry and mechanical properties. They compared the failure characteristic of DP600 galvanized sheets RSWs with that of DP780

galvannealed sheets. The DP600 galvanized steel failed by interfacial mode, whereas the DP780 galvannealed steel failed by button pull-out mode. Hayat *et al.* [25] have studied the effect of welding parameters on fracture toughness of galvanized DP600 automotive steel sheets RSWs. They concluded that the fracture toughness of RSW depends on the nugget diameter, sheet thickness, tensile rupture force, welding time, and current. Hernandez *et al.* [26] studied the behavior of dissimilar weldment of DP600 with other advanced high strength steels. They reported pull-out failure mode is observed when DP600 is welded to other advanced high strength steels, compared to DP600 steel.

In the current research, the microstructure and mechanical properties of resistance spot welded DP600 steel was analyzed. Different microstructures of various sites were analyzed according to their thermal history during welding process. Additionally, mechanical properties of welded spots were investigated through tensile-shear and cross-tensile tests as well as hardness testing. Fractography analyses were conducted to reveal the fracture mode.

2. Experimental Techniques

2.1. Material Characterization

The material used in this study, supplied by ThyssenKrupp Steel AG Division Auto (Essen, Germany), is cold rolled galvanized sheet of DP600 steel with 1.5 mm thickness. As can be seen from the chemical composition listed in Table 1, the material is a low carbon steel, with additions of a relatively high level of manganese, plus some Si and Cr to facilitate the formation of the dual phase microstructure and to offer the aimed properties.

Table 1. The chemical composition of the investigated DP steel- in weight-%.

C	Si	Mn	Cr	Mo	Al
0.09	0.2	1.24	0.14	0.2	0.026

The results of SEM (Figure 1) showed that the initial microstructures consisted of 85% ferrite and 15% martensite. The average ferrite grain size was 7 µm.

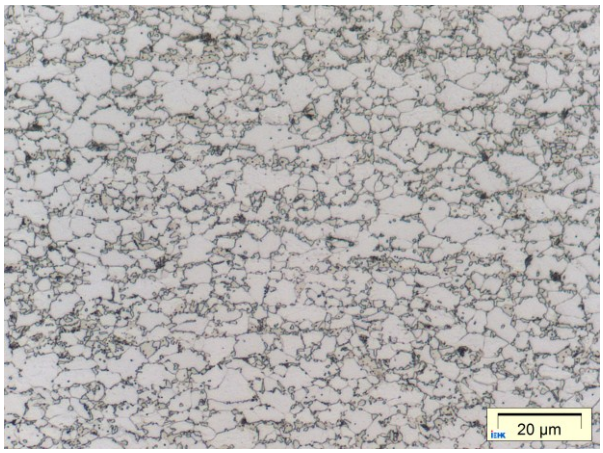

Figure 1. SEM picture of the studied base material.

2.2. Welding Experiment

The investigations were conducted on a C-shaped robot spot welding gun with a medium-frequency direct-current transformer (RWTH-Aachen University, Aachen, Germany). Water-cooled electrode caps of the G16 type according to DIN ISO 5821 were used for the welding tests, with a working surface of 6 mm.

Welding samples were prepared from cold rolled plates. The plates were machined into specimens of 83 × 45 × 1.5 mm^3 and finally they were welded together. The values of force, current, and time parameters used in this study are reported in Table 2. The parameter values were selected in such a way that, the minimum nugget diameter of $4*\sqrt{t}$, where t is the sheet thickness, was obtained after RSW and they were corresponded to welding parameters close to industrial conditions. For each sample, metallographic examination was carried out to reveal the microstructure. Tensile-shear, cross-tensile tests, as well as the hardness testing were applied to evaluate the mechanical properties. Three tensile-shear tests and three cross-tensile tests were performed.

Table 2. The operation conditions for RSW.

F_{EI} [kN]	Hold-back time [ms]	I_{S1} [kA]	t_{S1} [ms]
3	140	7	200

2.3. Thermocouple

The cooling rate has important influence on the formation of microstructure in the weld nugget and HAZ. To get thermal cycles of different places, three thermocouples Type K (chromel–alumel) were fixed at different distances from the weld spot. The distances were chosen to be 2.9, 3.5, and 4.3 mm, as shown in Figure 2. Thermocouples were situated on positions away from welding electrodes to inhibit the damage.

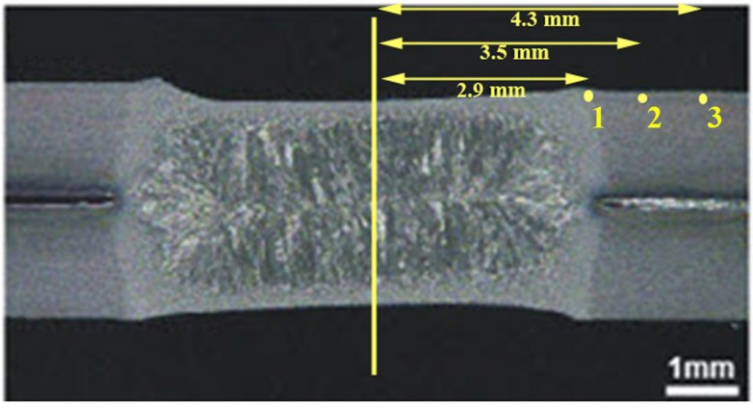

Figure 2. The location of the thermocouples.

2.4. Tensile Tests and Specimen Analysis

Tensile testing was carried out on a servo-hydraulic testing machine at room temperature. The static tensile tests for RSW welded specimens were performed at a speed of 5 mm/min in order to exploit the yield point of the materials in a better way. The geometries of the tensile-shear test specimen and the

cross-tensile test specimen are shown in Figure 3. In case of the tensile-shear test the testing direction is along the length of the welded specimen. For the cross-tensile test the testing direction is perpendicular to the plane of the welded specimen.

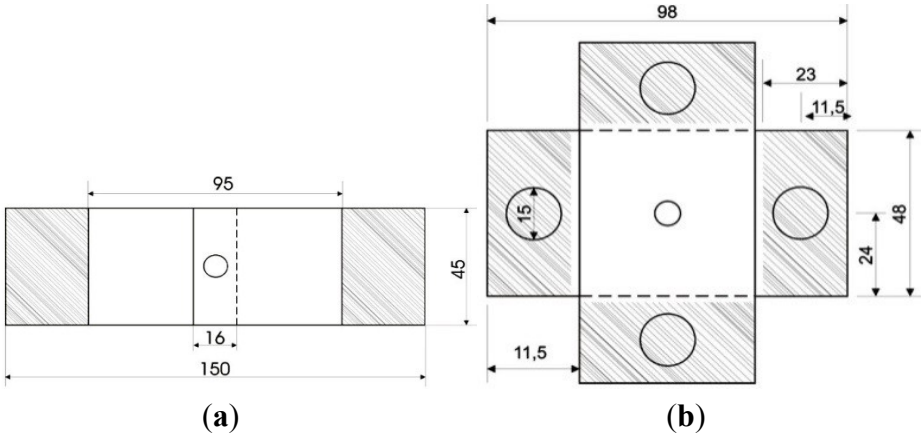

Figure 3. Specimen geometry: (**a**) tensile-shear test; and (**b**) cross-tensile test (The dimensions are all in mm).

Optical and scanning electron microscopes were applied to evaluate the macrostructure and microstructure as well as fracture surfaces. Etching was performed using 2% Nital solution. The Vickers microhardness test was performed using an indenter load of 1000 g and dwell time of 15 s to obtain a diagonal hardness profile. The hardness traverses were done normal to the faying surface.

3. Experimental Results and Discussion

3.1. Microstructure

Macrostructure of weld cross-section is shown in Figure 4. Three different zones are observed in Figure 4. Observed in the microstructure are: fusion zone (FZ), which is melted and re-solidified during the welding process and showing a cast structure with columnar grains, heat affected zone (HAZ), which is not melted but undergoes microstructural changes, and base metal (BM) which does not experience any microstructural changes.

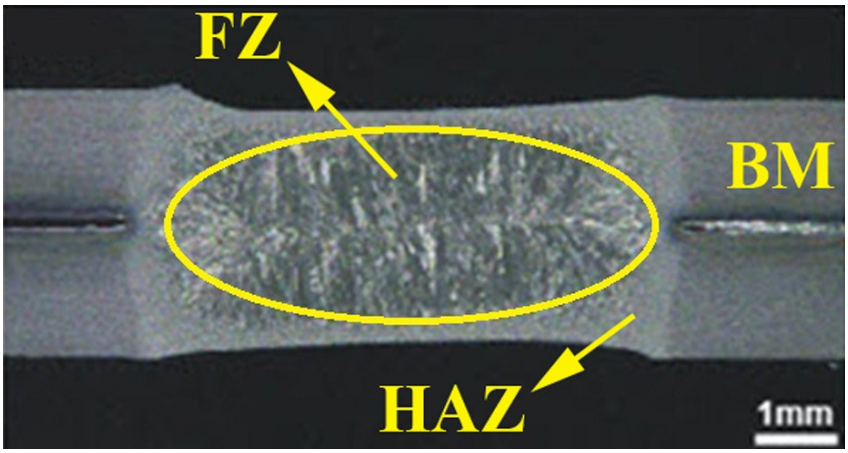

Figure 4. Macrostructure of DP600 RSW.

Microstructure of FZ and HAZ are depicted in Figure 5. Both have a martensitic microstructure, although FZ grains are columnar. This can be related to thermal and cooling regimes of these zones during welding. FZ is melted and HAZ is heated to above A1 temperature. Severe cooling rate of both zones results in martensite formation. Cooling rates of more than 400 °C/s have been reported for FZ and HAZ during RSW [17].

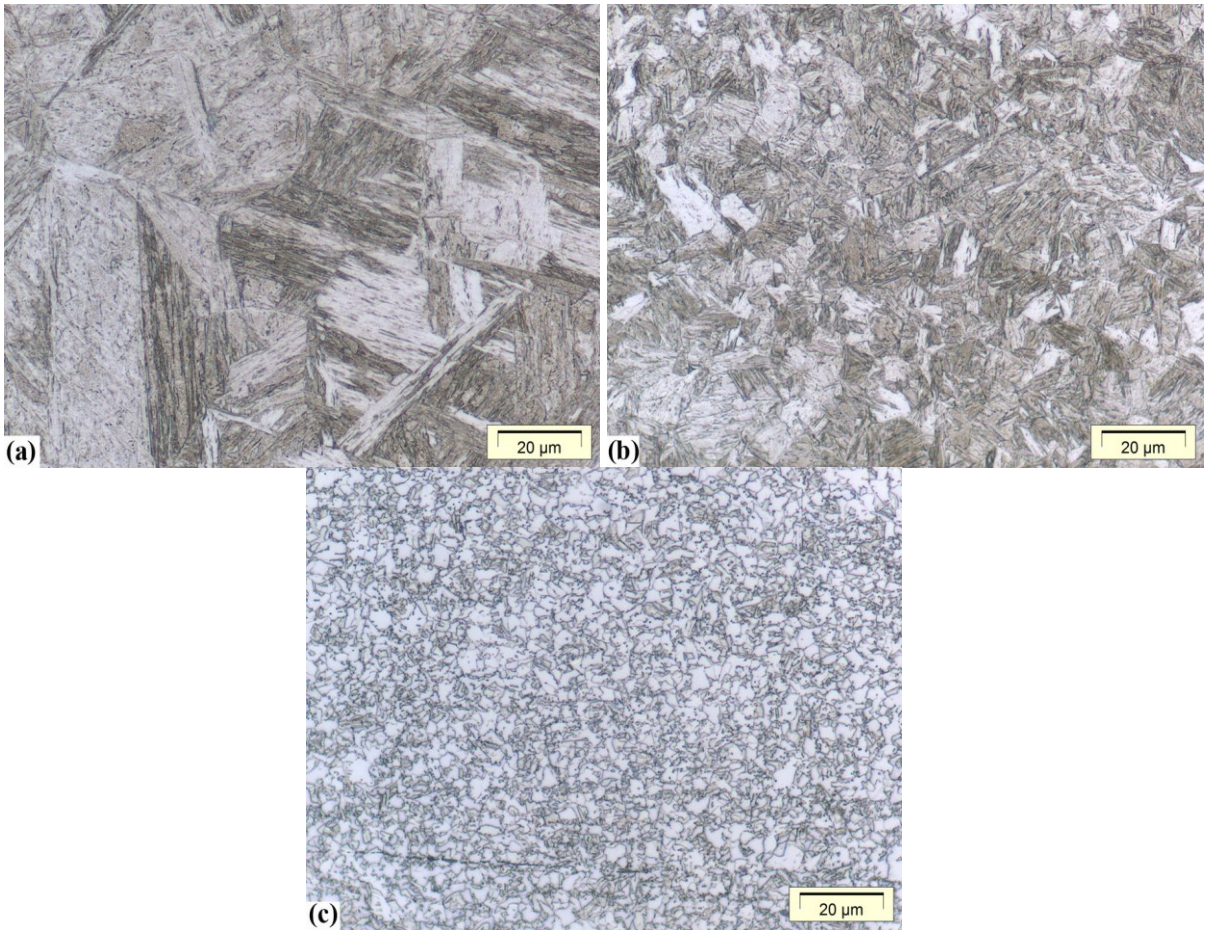

Figure 5. Microstructure of (**a**) fusion zone; (**b**) HAZ and (**c**) base metal.

Temperature history of applied thermocouples are presented in Figure 6. It is observed that for thermocouple in HAZ, temperature reaches to 900 °C and cooling rate is above 400 °C/s and for other thermocouples, located in BM and near the HAZ, the highest experienced temperature is below 600 °C. In RSW the cooling rate of welding is at a very high level. In the current case of 1.5 mm thickness, the cooling rate is estimated to be above 600 °C/s. These cooling rates are much higher than those needed to form martensite (which are around 40–120 °C/s) in the weld and HAZ in DP steels [27,28]. There is insufficient time for carbon diffusion at such high cooling rates. Obviously, the process with the above estimated cooling rates will lead to a significant amount of martensite in the fusion zone and HAZ. These zones are prone to the occurrence of brittle fracture.

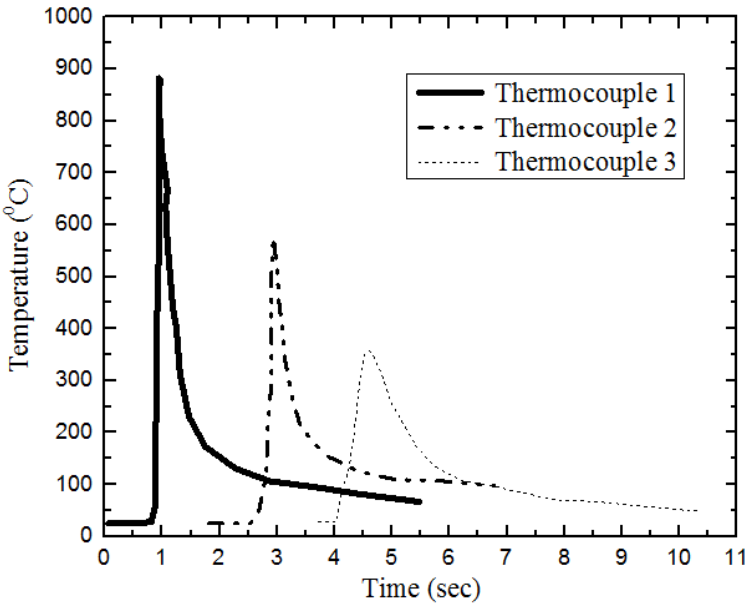

Figure 6. Temperature history of different thermocouples shown in Figure 2.

Regarding the above equation developed for estimation of austenitizing temperature [29], the austenization temperature for the studied steel is 870 °C. In this regard, HAZ temperature is above the austenization temperature, and during cooling, HAZ undergoes martensitic transformation, while temperatures of other zones away from HAZ are below A1 temperature and martensitic transformation does not occur. According to TTT diagram of DP600 steel (Figure 7) and measured cooling rates for HAZ and other sites, the former should have a martensitic microstructure and the latter should have a BM feature microstructure. Microstructures of these zones are presented in Figure 5. In the microstructure of the BM zone near HAZ (Figure 5c) is the presence of some carbide phases distributed in ferrite matrix is recognizable. This can be related to tempering of martensite base metal during RSW.

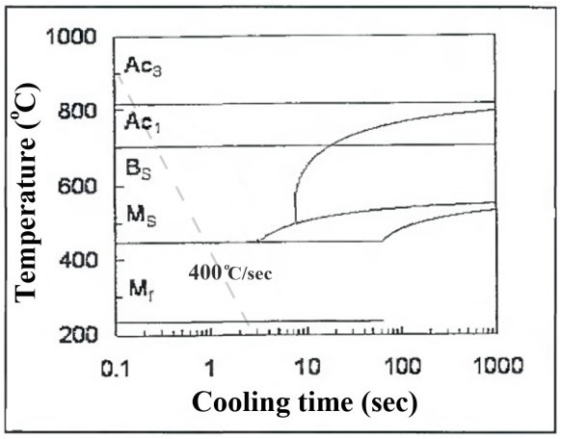

Figure 7. TTT diagram of the studied steel [28].

$$T_A\left[{}^0C\right] \approx 947 - 264\sqrt{\%C} - 8\%Mn + 45\%Si + 5\%Cr$$
$$+74\%Al + 10\%Mo - 23\%Ni + 94\%V$$

Hardness measurements are delivered in Figure 8. It is observed that hardness values of FZ and BM are about 400 HV and 200 HV, respectively, and hardness values of HAZ is about 310 HV. As hardness values more than 400–450 and 300–350 HV can be related to martensite and bainite phases, respectively, and hardness values less than 300 HV 0.8 can be attributed to ferrite phase [30], presence of martensite phase in HAZ and ferrite in BM is predictable, which is in agreement with metallographic observations. Low hardness of HAZ with respect to FZ can be related to high elastic distortion in the crystal volume of FZ grains. It is known that elastic distortion in the crystal resulting from martensitic transformation is a factor that enhances the hardness of martensite [31].

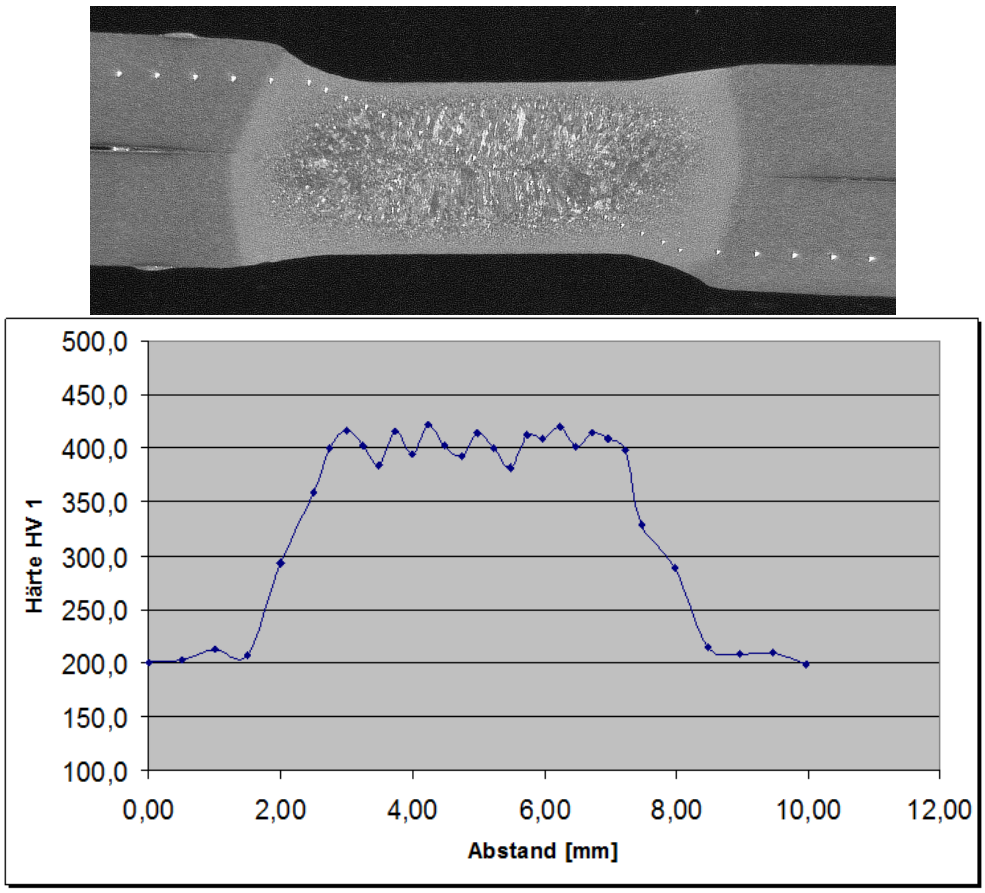

Figure 8. Hardness profile for the studied weldment.

The hardness map is very important to identify the mechanical properties of different developed zones in the welding. This would be necessary to study the effect of developed microstructures during welding on the final mechanical properties of the material [32,33]. Additionally, this map would be useful for evaluating the micromechanical properties of the material [32]. Surface hardness map of the welded structure is depicted in Figure 9. Inhomogeneity in hardness can be related to microstructure of different zones which are not homogenous. Non-homogenous distribution of allying elements during re-solidification in FZ and presence of different phases in HAZ and BM are numerated as the main parameters for inhomogeneity [34]. As it is observed in Figure 9 the hardness value of BM is about 200 HV and hardness values of FZ and HAZ are about 400 HV and 250–350 HV, respectively.

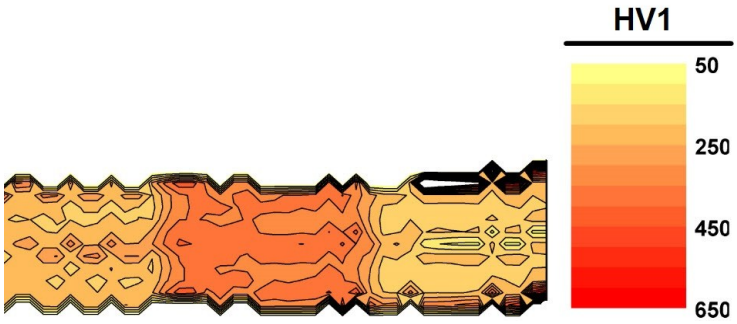

Figure 9. Surface hardness map of the studied weldment.

3.2. Mechanical Properties

The results for tensile-shear and cross-tensile tests are delivered in Figure 10. As it comes from Figure 10, the failure mode is pull-out and the fracture has initiated from a periphery point around the weld nugget. Based on the results in proceeding section, the pointed area has a martensitic microstructure. It is believed that stress concentration, due to electrode welding force, along the weld nugget periphery results in crack initiation in points which have a martensitic microstructure. As martensite is not a deformable phase, a ductile fracture is not expected.

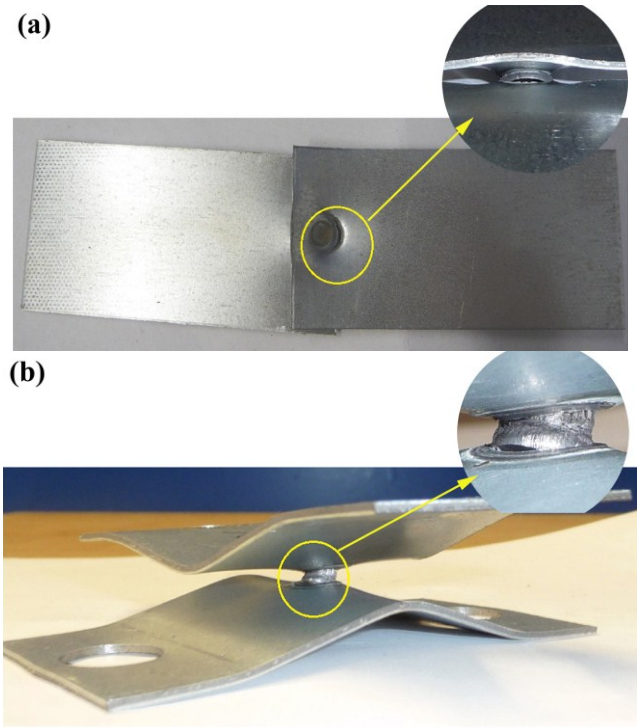

Figure 10. Specimens after (**a**) tensile-shear test and (**b**) cross-tensile test.

The fracture surface is shown in Figure 11. A brittle fracture surface is common characteristic of this surface. This may be related to low carbon content of the studied steel, which enhances the ductility and decreases the hardness and strength.

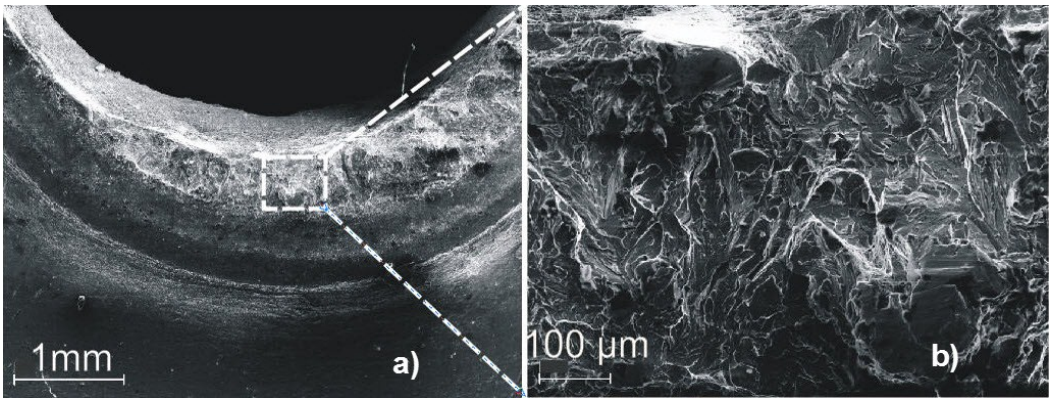

Figure 11. (**a**) Fracture surface of the resistance spot welded DP600 steel after cross-tensile test; (**b**) detailed appearance of the fracture surface shown in (**a**).

Load-displacement curves relating to tensile-shear and cross-tensile tests are shown in Figure 12. The mean load for failure for the cross-tensile samples is 6.8 kN, while the mean displacement is 11.5 mm. The mean displacement in case of cross-tensile tests is much higher than that of shear-tensile tests (the mean displacement for shear-tensile tests is 2.5 mm and the mean load for failure in case of tensile-shear test is 7.9 kN). In the current study the nugget diameter is approximately 4.5 mm.

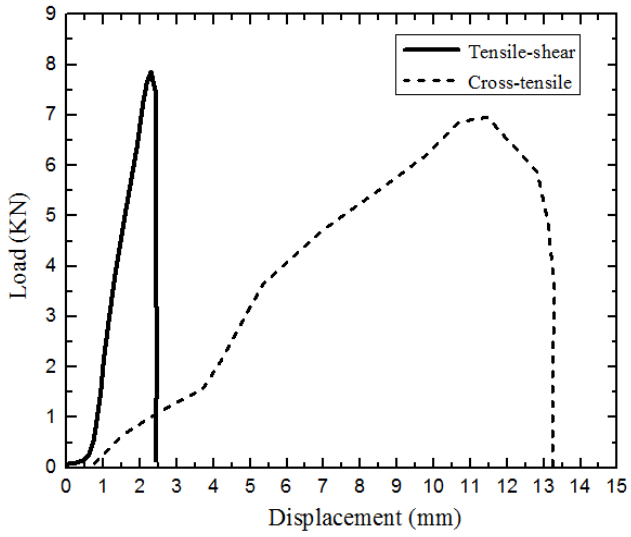

Figure 12. Load-displacement curves relating to tensile-shear and cross-tensile tests of the studied weldment.

4. Summary and Conclusions

- Characterization and mechanical properties of the welded joints was performed. Light optical and electron microscopy, hardness mapping, and tensile testing were used for this purpose.
- The fusion zone in the RSW weld consisted of a hard martensitic columnar microstructure with hardness of about 400 HV.
- HAZ consisted mainly of martensite, and other areas had a BM feature microstructure. Although, in microstructure of the BM zone near HAZ, the presence of some carbide phases distributed in ferrite matrix, as a result of tempering, was recognizable.

- Pull-out failure mode was the characteristic of fractured specimens, while the initial cracks were initiated from the periphery points around the weld region.
- Fracture surface analyses of the broken shear-tensile and cross-tensile specimens indicated a mainly brittle fracture surface; however, the presence of some deformation was observable in fracture surface.

Acknowledgments

The authors would like to acknowledge the funding and support from AiF (Arbeitsgemeinschaft industrieller Forschungsvereinigungen). This research was carried out in the framework of Project AiF 15548 N.

Author Contributions

Ulrich Prahl was the principle investigator of the research. Aydemir Abdurakhmanov, and Mahmoud Abbasi carried out the welding tests. Krishnendu Mukherjee characterized the microstructure of the welded samples. Ali Ramazani performed mechanical tastings, hardness map, fractography, and wrote the paper.

Conflicts of Interest

The authors declare no conflict of interest.

References

1. Davies, G. *Materials for Automobile Bodies*; Elsevier: Butterworth–Heinemann, UK, 2003.
2. Ramazani, A.; Mukherjee, K.; Prahl, U.; Bleck, W. Modelling the Effect of Microstructural Banding on the Flow Curve Behaviour of Dual-Phase (DP) Steels. *Comput. Mater. Sci.* **2012**, *52*, 46–54.
3. Ramazani, A.; Mukherjee, K.; Schwedt, A.; Goravanchi, P.; Prahl, U.; Bleck, W. Quantification of the Effect of Transformation-Induced Geometrically Necessary Dislocations on the Flow-Curve Modelling of Dual-Phase Steels. *Int. J. Plasticity* **2013**, *43*, 128–152.
4. Cornette, D.; Hourman, T.; Hudin, O.; Laurent, J.P.; Reynaert, A. High Strength Steels for Automotive Safety Parts. *SAE Trans. J. Mater. Manuf*. **2001**, *110*, 37–47.
5. Ramazani, A.; Ebrahimi, Z.; Prahl, U. Study the effect of martensite banding on the failure initiation in dual-phase steel. *Comput. Mater. Sci.* **2014**, *87*, 241–247.
6. Shaw, J.R.; Zuidema, B.K. New High Strength Steels Help Automakers Reach Future Goals for Safety, Affordability, Fuel Efficiency and Environmental Responsibility. *SAE Trans. J. Mater. Manuf.* **2001**, *110*, 976–983.
7. Mukherjee, K.; Ramazani, A.; Yang, L.; Prahl, U.; Bleck, W.; Reisen, U. Characterization of gas metal arc welded hot rolled DP600 steel. *Steel Res. Int*. **2011**, *82*, 1408–1416.
8. Ramazani, A.; Bruehl, S.; Gerber, T.; Bleck, W.; Prahl, U. Quantification of bake hardening effect in DP600 and TRIP700 steels. *Mater. Des.* **2014**, *57*, 479–486.

9. Wang, W.; Li, M.; He, C.; Wei, X.; Wang, D.; Du, H. Experimental Study on High Strain Rate Behavior of High Strength 600–1000 MPa Dual Phase Steels and 1200 MPa Fully Martensitic Steels. *Mater. Des*. **2013**, *47*, 510–521.
10. Abbasi, M.; Ketabchi, M.; Ramazani, A.; Abbasi, M.; Prahl, U. Investigation into the effects of weld zone and geometric discontinuity on the formability reduction of tailor welded blanks. *Comput. Mater. Sci.* **2012**, *59*, 158–164.
11. Ramazani, A.; Mukherjee, K.; Prahl, U.; Bleck, W. Transformation-Induced, Geometrically Necessary, Dislocation-Based Flow Curve Modeling of Dual-Phase Steels: Effect of Grain Size. *Metall. Mater. Trans. A* **2012**, *43*, 3850–3869.
12. Ramazani, A.; Mukherjee, K.; Quade, H.; Prahl, U.; Bleck, W. Correlation between 2D and 3D flow curve modelling of DP steels using a microstructure-based RVE approach. *Mater. Sci. Eng. A* **2013**, *560*, 129–139.
13. Ramazani, A.; Schwedt, A.; Aretz, A.; Prahl, U. Failure Initiation in Dual-Phase Steel. *Key Eng. Mater.* **2014**, *586*, 67–71.
14. Ramazani, A.; Mukherjee, K.; Abdurakhmanov, A.; Prahl, U.; Schleser, M.; Reisgen, U.; Bleck, W. Micro-Macro Characterisation and Modelling of Mechanical Properties of Gas Metal Arc Welded (GMAW) DP600 Steel. *Mater. Sci. Eng. A* **2014**, *589*, 1–14.
15. Reisgen, U.; Harms, A.; Ohse, P.; Schiebahn, A. Fracture Behaviour of Resistance Spot Welds on High-Strength and Higher-Strength Steels. *Weld. Cut.* **2009**, *8*, 148–151.
16. Ramazani, A.; Li, Y.; Mukherjee, K.; Prahl, U.; Bleck, W.; Abdurakhmanov, A.; Schleser, M.; Reisgen, U. Microstructure evolution simulation in hot rolled DP600 steel during gas metal arc welding. *Comput. Mater. Sci.* **2013**, *68*, 107–116.
17. Zhao, D.; Wang, Y.; Zhang, L.; Zhang, P. Effects of Electrode Force on Microstructure and Mechanical Behavior of the Resistance Spot Welded DP600 Joint. *Mater. Des.* **2013**, *50*, 72–77.
18. Shi, G.; Westgate, S.A. Resistance Spot Welding of High Strength Steels. *Int. J. Join. Mater.* **2004**, *16*, 9–14.
19. Zhang, H.; Wei, A.; Qiu, X.; Chen, J. Microstructure and Mechanical Properties of Resistance Spot Welded Dissimilar Thickness DP780/DP600 Dual-Phase Steel Joints. *Mater. Des*. **2014**, *54*, 443–449.
20. Ma, C.; Chen, D.L.; Bhole, S.D.; Boudreau, G.; Lee, A.; Biro, E. Microstructure and Fracture Characteristics of Spot-Welded DP600 Steel. *Mater. Sci. Eng. A* **2008**, *485*, 334–346.
21. Zhang, H.; Senkara, J. *Resistance Welding: Fundamentals and Applications*; Taylor and Francis CRC Press: Boca Raton, FL, USA, 2006.
22. Sun, X.; Stephens, E.V.; Khaleel, M.A. Effects of Fusion Zone Size and Failure Mode on Peak Load and Energy Absorption of Advanced High-Strength Steel Spot Welds. *Weld. J.* **2007**, *86*, 18s–25s.
23. Pouranvari, M.; Marashi, S.P.H. Failure Mode Transition in AHSS Resistance Spot Welds. Part I. Controlling Factors. *Mater. Sci. Eng. A* **2011**, *528*, 8337–8343.
24. Khan, M.I.; Kuntz, M.L.; Biro, E.; Zhou, Y. Microstructure and Mechanical Properties of Resistance Spot Welded Advanced High Strength Steels. *Mater. Trans.* **2008**, *49*, 1629–1637.

25. Hayat, F.; Ibrahim, S. The Effect of Welding Parameters on Fracture Toughness of Resistance Spot-Welded Galvanized DP600 Automotive Steel Sheets. *Int. J. Adv. Manuf. Tech.* **2011**, *58*, 1043–1050.
26. Hernandez, V.H.B.; Kuntz, M.L.; Khan, M.I. Influence of Microstructure and Weld Size on the Mechanical Behaviour of Dissimilar AHSS Resistance Spot Welds. *Sci. Tech. Weld. Join.* **2008**, *13*, 769–776.
27. Zhong, N.; Liao, X.; Wang, M.; Wu, Y.; Rong, Y. Improvement of microstructures and mechanical properites of resistance spot welded DP600 steel by double pulse technology. *Mater. Trans.* **2011**, *52*, 2143–2150.
28. Gould, J.; Khurana, S.; Li, T. Predictions of Microstructures When Welding Automotive Advanced High-Strength Steels. *Weld. J.* **2006**, *85*, 111s–116s.
29. Bleck, W. *Materials Sciecne of Steel*; Verlag Mainz: Aachen, Germany, 2007.
30. Naderi, M.; Ketabchi, M.; Abbasi, M.; Bleck, W. Analysis of microstructure and mechanical properties of different high strength carbon steels after hot stamping. *J. Mater. Process. Tech.* **2011**, *211*, 1117–1125.
31. Naderi, M.; Abbasi, M.; Akbari, A.S. Enhanced mechanical properties of a hot-stamped advanced high-strength steel via tempering treatment. *Metall. Mater. Trans. A* **2013**, *44*, 1852–1861.
32. Kalaki, A.; Ketabchi, M.; Abbasi, M. Thixo-joining of D2 and M2 tool steels: analysis of microstructure and mechanical properties. *Int. J. Mater. Res.* **2014**, *105*, 764–769.
33. Ramazani, A.; Pinard, P.T.; Richter, S.; Schwedt, A.; Prahl, U. Characterisation of Microstructure and Modelling of Flow Behaviour of Bainite-Aided Dual-Phase Steel. *Comput. Mater. Sci.* **2013**, *80*, 134–141.
34. Abbasi, M.; Naderi, M.; Akbari, A.S. Isothermal versus non-isothermal hot compression process: A comparative study on phase transformation and structure-property relationships. *Mater. Des.* **2013**, *45*, 1–5.